LCC-0140
SLAC-TN-04-041
June 2004

Linear Collider Collaboration Tech Notes

Sensitivity to Nano-Tesla Scale Stray Magnetic Fields

J. Frisch, T.O. Raubenheimer, P. Tenenbaum
June 2004

Stanford Linear Accelerator Center
Stanford University
2575 Sand Hill Road
Menlo Park, CA

Abstract: We consider the NLC's sensitivity to stray magnetic fields in the nanotesla regime.

Sensitivity to Nano-Tesla Scale Stray Magnetic Fields

J. Frisch, T. O. Raubenheimer, P. Tenenbaum
LCC-Note-0140
June 7, 2004

Abstract

We consider the NLC's sensitivity to stray magnetic fields in the nanotesla regime.

1 Introduction

The Next Linear Collider (NLC) requires a small vertical emittance and beam size in order to achieve its luminosity goals. As a result, the vertical beam position at the IP can be influenced by stray magnetic fields at the level of nanotesla. In this Note we characterize potential sources of stray fields via analytical methods and measurements in the field, and analyze their potential effect on the NLC beam in various regions.

1.1 Extremely Low Magnetic Fields

Under ordinary circumstances, stray magnetic fields can be addressed through the use of materials with a high coefficient of permeability μ. In these materials the fraction of the magnetic field which can be transmitted is proportional to $1/\mu$[1]. The steel alloys used for accelerator magnets, as an example, often have $\mu \approx 10^3$ [2], allowing considerable reduction of the magnetic field.

Magnetic shielding via high-permeability material relies on the applied field supplying the material with a sufficient density of magnetic energy to reorient the magnetization within the material. At some low level of magnetic field this requirement is no longer satisfied, leading to unshielded transmission of the magnetic field through the material. It is this amplitude-dependent behavior which makes microtesla and nanotesla fields so vexing to accelerator designers [3].

One other form of shielding is available for consideration. This is eddy-current shielding, which is the source of frequency-dependent skin depth in conductors. This method of shielding appears to remain valid for the lowest field levels of concern to accelerators, but is only effective for AC fields. Fortunately, as we shall see, AC fields are far more important than DC fields for the NLC. In this Note we will invoke eddy-current shielding as necessary but assume that permeability shielding is absent.

2 Stray Fields in the NLC Environment

We consider three primary sources of stray field in the NLC environment: natural fields (the earth's magnetic field and/or fields in ore deposits near the tunnel); fields associated with the high-power RF system (klystrons, modulators, modulator charging power supplies); and assorted technical fields not related to the RF system (including eddy currents in rebar used in construction of the tunnel walls).

It is important to note that not all stray fields are of equal importance to the NLC beam. For example, the steering from the very low frequency (DC to 0.001 Hz) component of the earth's field is not important: during operations this deflection will be eliminated by steering the beams into collision. Stray fields at frequencies between 0.001 Hz and approximately 1 Hz can be addressed as part of the linac steering and/or the train-by-train steering feedbacks in the linac if the fields

are not excessively large; for example, the IP feedback can probably provide acceptable damping of beam motions at 1 Hz which are several times as large as the RMS beam size [4]. Stray fields at the line frequency of 60 Hz will appear as a "time-slot" variation: a fixed variation between the odd-numbered and even-numbered bunch trains at the NLC's 120 Hz repetition rate. Since the variation between odd and even trains from 60 Hz noise does not change with time, one can apply a constant correction to either the odd or the even trains. The main requirement is that the bandwidth of the correction system be adequate for switching completely from one state to the other in the intra-train period of 8.3 milliseconds, but systems with this capability have been demonstrated on the SLAC linac [5]. Stray fields at the NLC's 120 Hz repetition rate are sampled by the beam at 120 Hz and thus appear as a DC offset. Odd harmonics of 60 Hz will appear to be "time-slot" variation and be corrected by the time-slot steering system described above. What remains important, therefore, is any AC stray field with a frequency above about 1 Hz and which is not at a harmonic, either odd or even, of 60 Hz.

2.1 Natural Stray Fields

In the frequency band above 0.1 Hz, ambient natural fields have an RMS variation of approximately 1 nanotesla. The spectrum of the fields follows a 1/f distribution, and therefore the RMS field above approximately 1 Hz should be below 0.1 nT [6].

2.2 Fields from the RF System

The high-powered RF system contains 3 components capable of driving magnetic fields: the klystron itself, the modulator, and the modulator's high voltage power supply ("charging circuit"). All of these components are housed in the equipment tunnel, which will likely be over 9 meters away from the accelerator housing.

An NLC RF unit contains 3 electric currents which can drive magnetic fields: the current from the high-voltage power supply which charges the capacitors in the modulator, which supplies about 40 amperes of DC current; the primary current from the mdoulator discharge, which is 6 kA and lasts about 2 microseconds; and the klystron current, which is about 500 amperes for 2 klystrons per modulator and lasts about 2 microseconds.

The largest field in this system will be driven by the 6 kA current in the modulator primary. In the worst case the modulator current is as close as possible to the accelerator (about 9 meters) and the current return is infinitely far away. In this case we can treat the field at the accelerator as being driven entirely by the 6 kA current and neglect the field from the current return. If we assume that the modulator is about 2 meters tall, we can use the Biot-Savart law to determine that, at a distance of 9 meters, the magnetic field from the modulator current is 15 μT.

Although 15 μT seems like a large field relative to the nT scal of natural stray fields, under steady-state conditions none of these currents should pose any concern for the NLC. All of these sources are either DC or synchronous with the beam's 120 Hz repetition rate, and thus will "appear" to be DC to the beam. The condition under which a deflection can occur is when an RF unit is switched between normal and standby timing, or else is switched on or off between bunch trains. Each of these breaks the time symmetry between the RF system and the beam.

The same basic pattern of low DC charging current, high pulsed modulator current, and moderate pulsed klystron current is reproduced in the lower-frequency RF systems in the NLC injectors, bunch compressors, pre-linacs, and crab cavity systems. The pulse duration and peak current values will be somewhat different from those described here.

2.3 Stray Fields from Non-RF Technical Sources

This category is a catch-all for sources that accompany the construction of a large accelerator complex at an otherwise natural site. This can include pumps and motors which are not operating synchronously with the 60 Hz line frequency (the SLC was notoriously plagued by mechanical pumps with a characteristic frequency of 59 Hz), magnet power supply or electronics sources, eddy currents in the rebar which supports the concrete walls of the housing, etc. In general it is unlikely that any attempt to categorize these *a priori* will succeed, and thus measurements are required.

Figure 1 shows the power spectrum of the stray fields measured in SLAC's End Station B (ESB) building. The building contains a large number of magnet power supplies, a substantial amount of 60 Hz AC power distribution equipment, and several klystron/modulator combinations. It is, in short, a reasonable representative of an accelerator environment, including fields from the RF systems. The measurements were performed at a location chosen at random in ESB, which is unlikely to be unusually bad or unusually good.

Figure 2 shows the integrated spectrum of the fields in ESB. The large steps in the integral at 60 Hz and 180 Hz are due to AC power and the modulators, which operate at 60 Hz. Since harmonics of 60 Hz are not expected to cause time-varying deflections, Figure 3 shows the integrated spectrum with 60 Hz, 120 Hz, and 180 Hz peaks excluded from the integration. While the total field in ESB is about 3 nT, 1 nT is driven by the calibration tone used in the measuring apparatus (the step at 1 Hz). Of the remainder, about 1.5 nT appears to be from 20 Hz sources, which might be 1200 RPM motors of various kinds (such as fan motors for cooling power supplies or air circulation).

3 Response of the NLC Beam to Stray Fields

The various regions of the NLC are not all equally sensitive to various forms of stray fields. We consider the individual regions below.

3.1 A Note on Methodology

The tightest tolerance on beam motion in the NLC is at the interaction point. In order to maintain full luminosity, an RMS beam jitter of 0.5 σ_y^* is permitted. For the 500 GeV CM parameters, this corresponds to an RMS jitter of about 1.5 nm.

Given the above, there are two mathematically-identical methods for calculating the severity of a deflection. One method is to calculate the amount of beam jitter, in nm, which will occur at the interaction point; this is equivalent to calculating the ratio between the applied magnetic field and the resulting beam motion (in m/T, for example). The alternate method is to calculate the amount of beam jitter, in sigmas, caused by a disturbance. The key to this latter technique is that, depending on the phase of the disturbance, a deflection of n sigmas somewhere in the NLC will be transformed to a deflection between 0 and n sigmas at the IP. As a general rule, we will use the IP sensitivity calculation for ambient fields, and report a sensitivity in m/T, and use the jitter in sigmas calculation for deflections from changes in RF complement.

3.2 Beam Delivery System

The beam delivery is located far from the RF power systems, and therefore klystrons or modulators switching their timing or other status will not have much impact in this region. The single high-power RF system in beam delivery is the drive for the crab cavity, but since the crab cavity is essential for delivering luminosity, we can neglect the impact of an unexpected trip of the crab

cavity klystrons (since such a trip will already ruin the luminosity, we do not need to worry that the resulting beam deflection will further degrade it).

Other natural or technical stray fields, on the other hand, are a more serious problem due to the optical design of the BDS. The BDS requires large vertical betatron functions (or equivalently small angular divergences), which means that a small deflection can be a large fraction of $\sigma_{y'}$, which translates to a large fraction of σ_y^*. More mathematically, we can define a point-sensitivity function, $F(s)$, as follows:

$$F(s) \equiv 0.3\frac{\mathrm{GeV}}{\mathrm{T.m}}\frac{1}{E_{\mathrm{beam}}}\sqrt{\beta(s)\beta^*}\sin(\psi^* - \psi(s)). \tag{1}$$

The function $F(s)$ for the NLC BDS at 250 GeV is plotted in Figure 4. Note that $F(s)$ has dimensions of inverse magnetic field (in this case, T^{-1}). To find the lattice sensitivity to a uniform stray field, we can integrate $F(s)$ over the length of the beamline. This leads to a lattice sensitivity of -0.172 m/T.

More realistically, the stray fields in the beam delivery system will have some spatial variation to them. Let us consider a stray field which is purely sinusoidal with wave number k and phase ϕ, $B = B_0\cos(ks - \phi)$. The displacement of the beam due to this sinusoidal magnetic field is given by:

$$\begin{aligned}\Delta y^*(k,\phi) &= \int F(s)B(s)ds \\ &= 0.3\frac{\mathrm{GeV}}{\mathrm{T.m}}\frac{1}{E_{\mathrm{beam}}}\int dsB_0\cos(ks-\phi)\sqrt{\beta(s)\beta^*}\sin(\psi^*-\psi(s)).\end{aligned} \tag{2}$$

For simplicity of presentation, let us define $\phi_{\max}(k)$ as the value of ϕ which maximizes Δy^* for a given wave number k. We can then define a lattice response function $G_1(k)$ thusly:

$$\begin{aligned}G_1(k) &\equiv \frac{\Delta y^*(k,\phi_{\max}(k))}{B_0} \\ &= 0.3\frac{\mathrm{GeV}}{\mathrm{T.m}}\frac{1}{E_{\mathrm{beam}}}\int ds\cos(ks-\phi_{\max}(k))\sqrt{\beta(s)\beta^*}\sin(\psi^*-\psi(s)).\end{aligned} \tag{3}$$

As a final complication, we note that while $G_1(k)$ shows the expected motion of a single beam under the influence of AC stray fields, the more crucial problem is the differential motion of the electron and positron beams at the IP. For this we define the analogous function $G_2(k)$. Note that the oscillation phase which maximizes the single-beam offset (and is thus the phase used to define G_1) may not be the phase which maximizes the beam-beam offset (which defines G_2).

Figure 5 shows G_1 and G_2 as functions of k. For small values of k, G_1 asymptotically approaches the aforementioned value of 0.172 m/T for uniform field, while G_2 approaches zero since the two beams are both driven in the same direction by a uniform magnetic field. The peak value of G_1 occurs at a wavelength of about 600 meters, corresponding to stray fields which are resonant with the betatron oscillation; the sharp minimum in G_2 at this value is again a result of the two beams being driven in the same direction.

In order to correctly estimate the amount of beam motion driven by stray magnetic fields, it is necessary to obtain a two-dimensional power spectrum $P(\omega,k)$ which correctly estimates the power density of the magnetic field component with frequency ω and wave number k. We can use the techniques developed for wavelike ground motion [7] to show that the expectation value for the beam-beam offset is given by:

$$\sigma^2_{\mathrm{beam-beam}} = \int_0^\infty \frac{d\omega}{2\pi}\int_0^\infty \frac{dk}{2\pi}P(\omega,k)B(\omega)\frac{G_2^2(k)}{2}, \tag{4}$$

where $B(\omega)$ is the power-damping capacity of the steering feedbacks as a function of frequency, and the factor of 2 in the response function term is due to the presumed random phase of the magnetic field with respect to the worst-case phase. At the moment only a one-dimensional power spectrum, Figure 1, is available. It is worth noting, however, that the maximum value of G_2 is 2.8 m/T. If the power spectrum $P(\omega, k)$ was a Dirac delta function in wave number at $k = 8 \times 10^{-3}$ (corresponding to the peak value of G_2), and if all of the frequency content was outside the range of correction of the feedbacks, and if the 20 Hz component of the field in Figure 3 was not corrected by engineering, then the expected RMS beam-beam offset would be about 1 σ_y^*. Since it is extremely unlikely that all of these conditions will be met, we anticipate that the beam-beam offset from stray fields in the beam delivery system will be significantly smaller than 1 σ_y^*.

3.3 Main Linac

In the case of the main linac, non-RF stray fields are much less of an issue. Figure 6 shows $G_1(k)$ for the main linac. The peak value is 0.056 m/T, which can be combined with the integrated spectrum in Figure 3 to yield an expected AC deflection of about 0.11 nm, far below 1 σ_y^*. The key concern in the main linac is therefore variation in the magnetic field driven by changes in the klystron complement.

The most potentially serious source of beam deflection is the 6 kA current in the modulator. The current pulse is approximately a square wave with 2 μs duration. In order to estimate the deflection, we must first estimate the shielding effect of the steel cabinet which encloses the modulator.

3.3.1 Eddy Current Shielding

The frequency-domain representation of a square pulse with duration t_0 is given by:

$$F(\omega) = \frac{1}{2\pi\omega} \left[\sin(\omega t_0) + i\left(1 - \cos(\omega t_0)\right)\right]. \tag{5}$$

The magnitude of F for $t_0 = 2\mu$sec is plotted in Figure 7. In the limit of low frequencies the magnitude reduces to $t_0/2\pi$ or approximately 31.8 nsec, and the first null of F occurs at $\omega = 2\pi \times 0.5$ MHz.

Within a conductor, the eddy-current shielding reduces the magnitude of the magnetic field according to [1]:

$$H_c = H \exp(-x/\delta) \exp(ix/\delta), \tag{6}$$

where δ is the skin depth,

$$\delta \equiv \sqrt{\frac{2}{\mu\omega\sigma}}. \tag{7}$$

The magnetic field generated by the modulator pulse is shielded by the cabinet surrounding the modulator, which is made of steel. The resulting field pulse is further shielded by the wall of the copper RF structure and the steel vacuum chambers in the linac quads. Let us assume that the modulator cabinet is 2 mm thick, that the vacuum chambers in the linac are 1 mm thick, and that both materials have a conductivity comparable to elemental iron, specifically $10^7\ \Omega^{-1}\ \mathrm{m}^{-1}$. The walls of the RF structure are copper, with a conductivity of $6 \times 10^7\ \Omega^{-1}\ \mathrm{m}^{-1}$; the thickness of the copper is difficult to estimate due to the complicated shape of the structure when the damping manifolds and their slots are included, so for purposes of calculation we have used a lower bound value of 8 mm, which is the approximate thickness of the copper wall at the location of a damping manifold. This is probably a serious underestimate since by design the damping manifolds are cut off from the accelerating cavities for frequencies below about 14 GHz. Finally, the linac has a

filling factor of 80%, meaning that 80% of the length is filled with RF structure and 20% with steel vacuum chambers of various kinds. For the time being we neglect the additional shielding from the bodies of the quadrupoles. Figure 8 compares the frequency characteristics of the modulator pulse with the magnetic field pulse outside the modulator cabinet, the pulse filtered by the modulator cabinet and the vacuum chamber, and the pulse filtered by the modulator cabinet and the RF structure. The latter 3 signals, converted back to the time domain, are shown in figure 9, relative to the amplitude of the unfiltered field. The linac is 80% RF structure and 20% steel vacuum chamber; Figure 10 shows a "z-weighted" mean of the field in the beamline. The peak filtered field is 0.34% of the unfiltered field, and is delayed by approximately 19 μsec relative to the unfiltered field.

3.3.2 Kick from Modulator Current

Let us consider the kick imparted to the beam by the activation of a previously-inert modulator at the low-energy (7.87 GeV) end of the main linac. The modulator is assumed to be in the equipment tunnel at a s location which places it next to the first y-focusing quad in the main linac. If the modulator is approximately 2 meters tall and the point of closest approach is 9 meters, we can use the Biot-Savart law to compute the magnetic field as a function of s (where we have arbitrarily defined $s = 0$ to be the longitudinal coordinate of the modulator):

$$B(s) \approx \frac{\mu_0 I_{\text{eff}}}{4\pi} \frac{18 \text{ m}^2}{(s^2 + 81 \text{ m}^2)^{3/2}}, \tag{8}$$

where I_{eff} is the effective current outside the cabinet shielding, approximately 0.34% of 6 kA or 20.4 amperes. Equation 8 shows that the peak field experienced by the beam should be around 50 nT, and that the deflection from the modulator current will act over an s distance long compared to the quad spacing at the upstream end of the linac, and therefore the beam energy gain versus s and its betatron phase advance over the afflicted area must be considered. Figure 11 shows the evolution of the deflection as the beam travels away from the modulator, normalized to the beam angular divergence. The deflection saturates at about 0.022 $\sigma_{y'}$. By symmetry we expect the deflection from $s < 0$ to be roughly equal to the deflection from $s > 0$, leading to a total deflection of 0.044 $\sigma_{y'}$ for 1 modulator suddenly springing into action. The kick from the klystron beam current will be much smaller, both because the klystron beam current is much smaller than the modulator current and because the klystron body is a thick wall of copper which will provide much better eddy-current shielding than the modulator cabinet.

It is important to note that in normal operation we can expect the RMS beam jitter from changes in the klystron complement to be much less than the aforementioned 0.044 σ, for 4 reasons. First, we expect that the klystron complement will remain stable in each linac for periods of about 1 second, meaning that only on 1 or 2 pulses out of 120 will the klystron complement change. Second, the 0.044 σ figure calculated above is for a modulator at the injection energy of 7.87 GeV, and the magnitude of the kick will vary as $1/\sqrt{E_{\text{beam}}}$. Third, we have calculated the skin depth of the modulator cabinet assuming $\mu = \mu_0$; in actuality the cabinet will almost certainly be some form of steel, so that the higher permeability of the material will give some additional reduction in the skin depth and therefore extra shielding. Fourth and most important, the modulator cabinet delays the peak of the deflecting field by about 19 microseconds compared to the timing of the modulator current. Since the modulator is next to the section of beamline that it powers, the modulator's current pulse has to be no more than a few hundred nanoseconds prior to arrival of the beam at the adjacent section of beamline. Therefore the deflecting field will not appear until several microseconds after the beam has already passed by.

3.4 Pre-Linac

The pre-linac is a 6 GeV linac placed between the first and second bunch compressors, which increases the beam energy from 2 GeV to 8 GeV. The pre-linac is qualitatively similar to the main linac, but with quantitative differences: a lower accelerating frequency (2856 MHz rather than 11.4 GHz), RF system pulse parameters which are matched to the lower frequency (5.0 μsec pulse width and 160 ampere klystron current, 6 kA modulator current [8]), and a different quad spacing (4 and 8 meters rather than 6, 12, and 18 meters).

The main qualitative difference is that the pre-linac is housed side-by-side with the 2 GeV linac used to accelerate the beam from the source to the damping ring. The two linacs accelerate beams in opposite directions, and both have spare RF units which are switched in timing between "standby" and "on" states on a pulse-by-pulse basis as needed. The total time over which beam is present in either of the two linacs is under one microsecond, which is short compared to the 5 microsecond modulator pulse. We can therefore make the approximation that all of the modulators for both linacs which are in the "on" timing must begin to discharge their currents several microseconds before any beam is present in the pre-linac, and all of the modulators which are in the "standby" timing will begin to discharge long after the beam has departed.

3.4.1 Ambient and Non-RF Technical Sources

Figure 12 shows the G_1 function for the pre-linac. The peak value is 0.045 m/T for fields with a wavelength of 85 meters. This will lead to negligible deflections at the IP if the NLC in-tunnel ambient field is held to the levels shown in Figure 3.

3.4.2 Changes in RF System Complement

Figure 13 shows the field versus time expected at the beamline given a unit field pulse of 5 μsec duration inside the modulator cabinet, and assuming a combination of cabinet shielding and either RF structure shielding or steel vacuum chamber shielding. Figure 14 shows the "z-averaged" field versus time. In the pre-linac the packing fraction is somewhat larger (almost 90%) and the walls of the structure somewhat thicker (about 1 cm) compared to the main linac. The shielding reduces the peak field to 0.44% of the unshielded value and delays the peak by 21 microseconds relative to the modulator pulse. The kick from an RF station cycling at the most-sensitive point in the pre-linac will produce a 0.17 $\sigma_{y'}$ deflection. As with the main linac, this is a very conservative estimate, and the RMS jitter contribution from RF station cycling in the pre-linac area will be far smaller than this.

3.5 Damping Rings

Time-varying stray fields at the level described in previous sections will have no effect on the damping rings. The focusing lattice in the damping rings is much stronger than the lattice in any other portion of the NLC, which makes the beam in the ring relatively immune to deflecting fields. In addition, the damping ring is far from the pulsed RF systems of the linacs.

3.6 Main Linac Bypass Lines

The main linac bypass lines are installed side-by-side with the main linac, separated from the latter by approximately 30 cm. The bypass lines permit operation at CM energies below full energy with high luminosity by allowing the beams to be accelerated to a relatively low energy and removed from the linac without passing through deactivated RF structures, thus limiting the emittance

dilution due to wakefields. Extraction points are provided to permit beam energies as low as 39 GeV and as high as 250 GeV to be transported in the bypass line.

Figure 15 shows the horizontal betatron function for the bypass lines in its lowest- and highest-energy configurations. The lowest energy configuration transports 39.4 GeV electrons with a phase advance per cell of 117 degrees, while the highest energy configuration transports 250 GeV electrons with a phase advance per cell of 15.6 degrees.

When the bypass lines are in use the neighboring sections of the main linac are deactivated, and therefore the RF-related fields are not present. The only concern for the bypass lines is ambient and/or non-RF technical stray fields.

Figure 16 shows G_1 for the 39.4 GeV/beam bypass line. At a wavelength of about 660 m the stray fields are near the betatron wavelength of the line in this configuration leading to a maximum response at the IP of 6.2 m/T. Figure 17 shows G_1 for the 250 GeV/beam bypass line. In this higher-energy configuration the maximum value of G_1 occurs at a wavelength of about 5 km, with a response of almost 1 m/T.

3.7 Polarized Positron Transfer Line

In the event that a polarized positron source is used at the NLC, it will be necessary to transport the positrons from the 150 GeV point on the electron side of the collider to the pre-damping ring injection point at the far end of the positron side of the collider. This will be accomplished with an appropriate FODO lattice running across the site.

It is expected that the positrons will be accelerated to 2 GeV near their production point and then transported to the PPDR in a long, sparse lattice similar to the bypass line. We can scale the response of the 39 GeV bypass line to that of the positron transfer line by considering the following factors:

- The transfer line will probably be about twice as long as the bypass line, and at the wave number which generates the strongest response the response should scale linearly with the system length.
- The beam energy will be reduced by a factor of about 20, and the response will scale inversely with this energy.
- The betatron function at PPDR injection will be larger than the NLC IP by a factor of about 5 orders of magnitude, and the response will scale with the square root of this factor.

The factors listed above suggest that the positron transfer line's peak response will be about 7.8×10^4 m/T. The undamped positron bunch has a normalized emittance of approximately 10^{-2} m.rad, an energy of 2 GeV, and a betatron function around 10 meters, for an RMS size of roughly 5.1 mm. This implies that 65 nT are needed to generate a 1 sigma orbit change at injection, far more than what is seen in ambient field measurements.

The transfer line would also be potentially influenced by changes in main linac klystron complement. Here the problem is simpler to solve since the quad spacing and betatron functions are large, with the result that it is a reasonable approximation to state that the entire kick from a modulator is applied at a point. The integrated kick of the modulator, including both the vacuum chamber and the cabinet shielding, sums to approximately 4.4×10^{-6} T.m. For a 2 GeV beam this would amount to a deflection of 0.67 μrad, and assuming a β_y value of 450 meters and normalized emittance of 10^{-2} m.rad, this constitutes a kick of less than 0.1% of $\sigma_{y'}$.

4 Conclusion

We have considered the sensitivity of assorted regions in the NLC to time-dependent variations in the local magnetic field. Two sources of stray field were considered: fields from changes in the complement of RF sources (klystrons and modulators) presently in use, and fields from non-RF technical sources (power supplies, fan motors, etc.). The fields from the former can be calculated from Maxwell's equations, while the latter must be measured *in situ.* A set of test measurements from SLAC's End Station B were used to represent these.

The regions considered were the transfer line for undamped positrons, the damping ring, the prelinac, the main linac, the linac bypass lines, and the beam delivery system. In no case was it found that fields from changes in the RF complement produced unacceptable deflections. In the case of the bypass lines and the beam delivery system the sensitivity is such that ambient technical sources of stray field may produce unacceptable deflections at the IP, but that a "conspiracy of errors" is required; specifically, the power spectrum of the ambient technical fields must be concentrated at the wavelength which produces the greatest response for each system, and at the frequencies which are not amenable to correction by beam-based feedbacks. The principal remaining unknowns are twofold:

- Is ESB a reasonable representation of a beamline housing? At present ESB is occupied by the NLC Test Accelerator (NLCTA), which includes several modulators and a vast number of magnet power supplies, many of which are supplied with cooling fans. In addition the building has several large and powerful fans used for ventilation. Additional measurements in more representative sites, such as the Final Focus Test Beam (FFTB) housing are in the planning stage.

- The most severe deflections in the bypass line and BDS cases require a "conspiracy of errors," specifically that the spatial variation of the deflecting fields must have the correct amplitude and phase to produce the maximum beam-beam offset at the IP. A more realistic estimate would take into account the spectrum of the ambient field as a function of wave number. Measurements of the two-dimensional power spectrum $P(\omega, k)$ are planned for the near future.

References

[1] J.D. Jackson, *Classical Electrodynamics,* Second Edition, 201 (1975).

[2] J. Tanabe, private communication (2001).

[3] N.J. Walker, `http://www.ligo.caltech.edu/~donna/Walker_talk.pdf`, 49-50 (2004).

[4] L. Hendrickson *et al*, "Implementation of Dynamic Misalignments and Luminosity Stabilization," *Proceedings of the IEEE Particle Accelerator Conference* (2003).

[5] L. Hendrickson *et al*, "Feedback Systems for Linear Colliders," *Proceedings of the IEEE Particle Accelerator Conference* (1999).

[6] `http://www.ips.gov.au/Main.php?CatID=8&SecID=3&SecName=Magnetic%20Field&SubSecID=1&SubSecName=Geomagnetic%20Activity&LinkName=Geomagnetic%20Pulsations%20in%20Aeromagnetic%20Surveys`.

[7] J. Irwin, F. Zimmermann, "Impact of Final Focus Ground Motion on NLC Luminosity," *Proceedings of the 5th European Particle Accelerator Conference* (1996).

[8] R.S. Larsen, "Technical Systems Configuration – Electrical, Klystrons/Modulators" (2001).

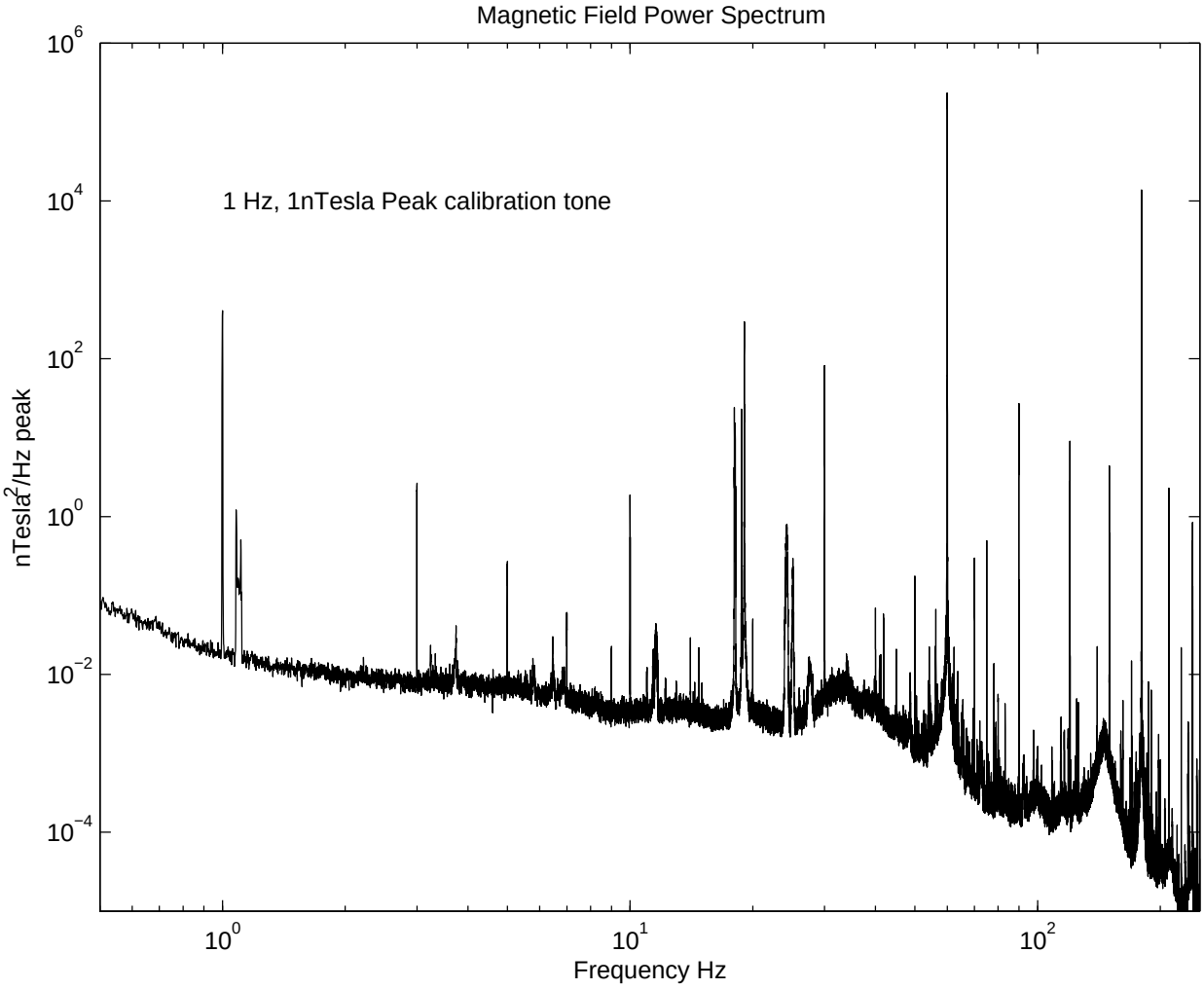

Figure 1: Ambient magnetic field spectrum measured in SLAC End Station B..

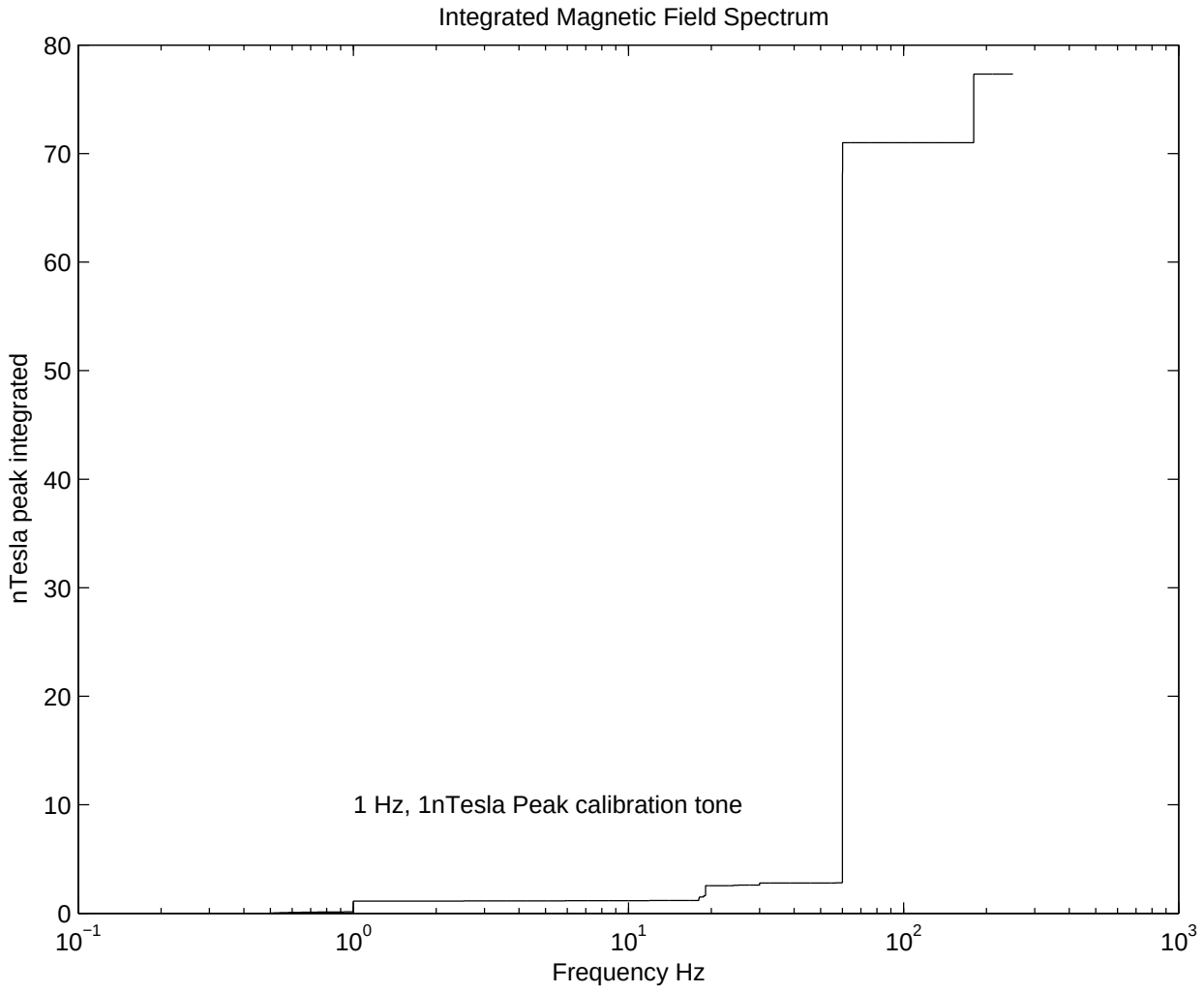

Figure 2: Integrated magnetic field in End Station B.

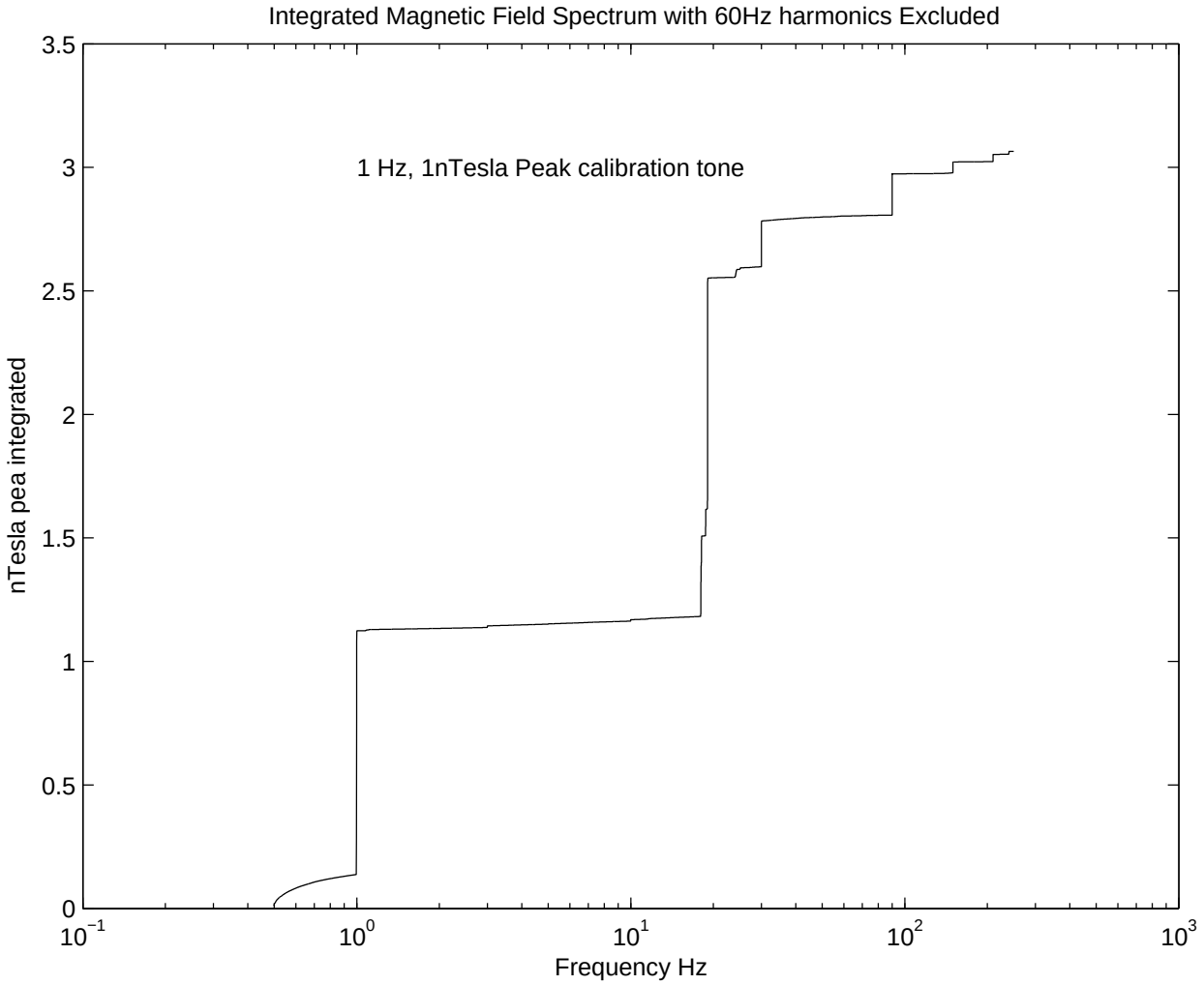

Figure 3: Integrated magnetic field in End Station B, with harmonics of 60 Hz suppressed.

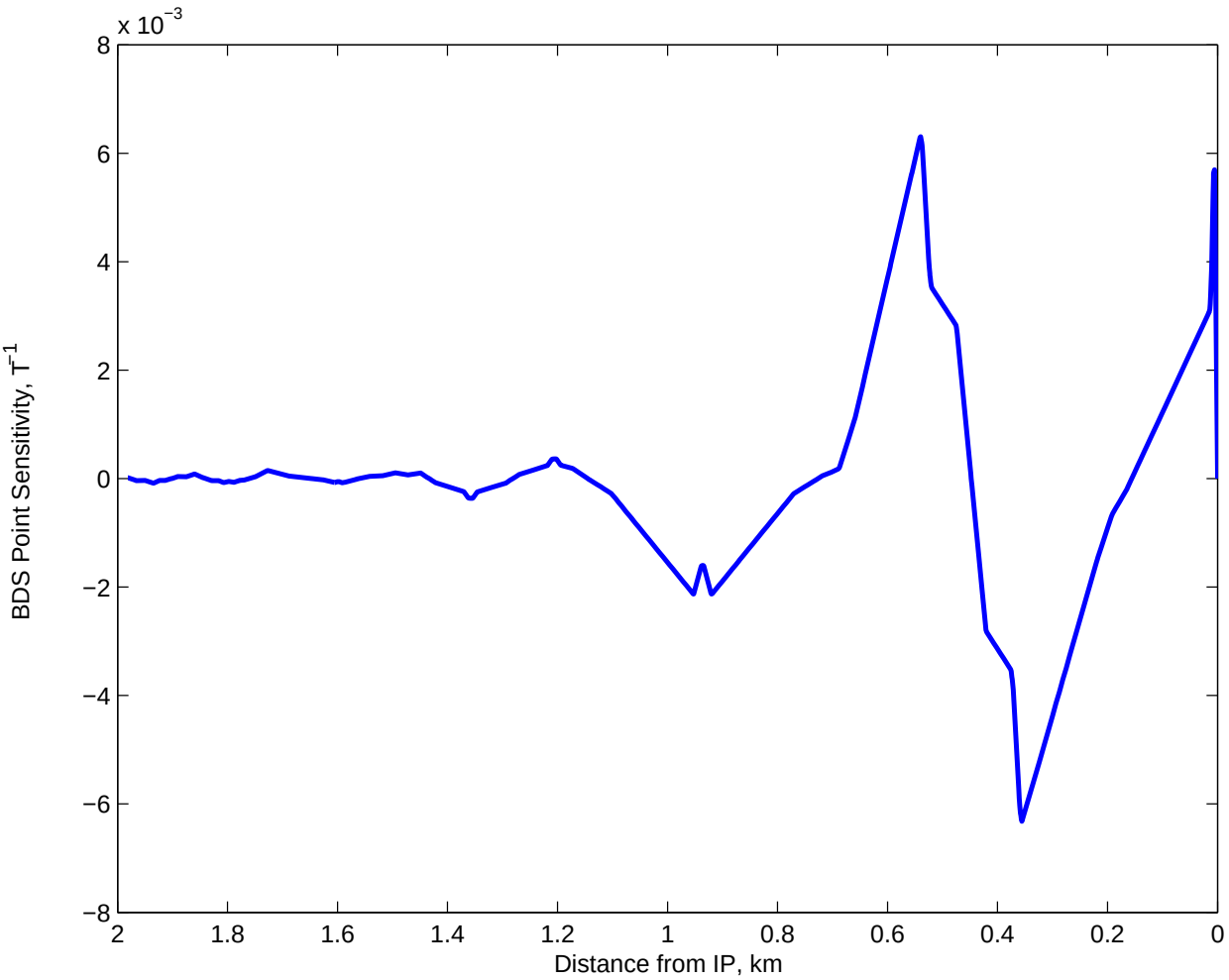

Figure 4: Point-sensitivity function for the NLC BDS at 250 GeV.

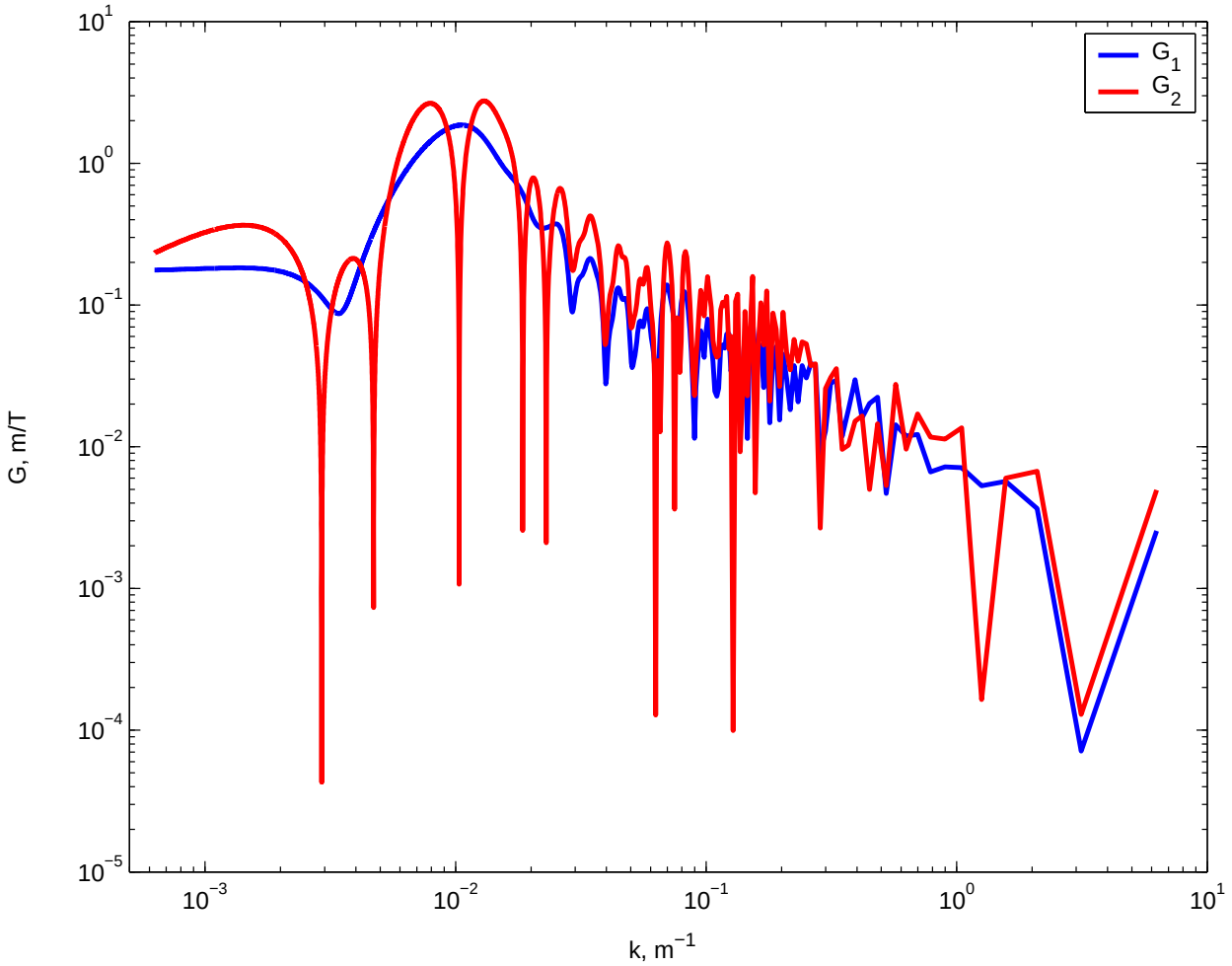

Figure 5: Sensitivity of IP beam position to a magnetic field with wave number k applied in the BDS. Single beam offset (blue) and beam-beam offset (red) are shown.

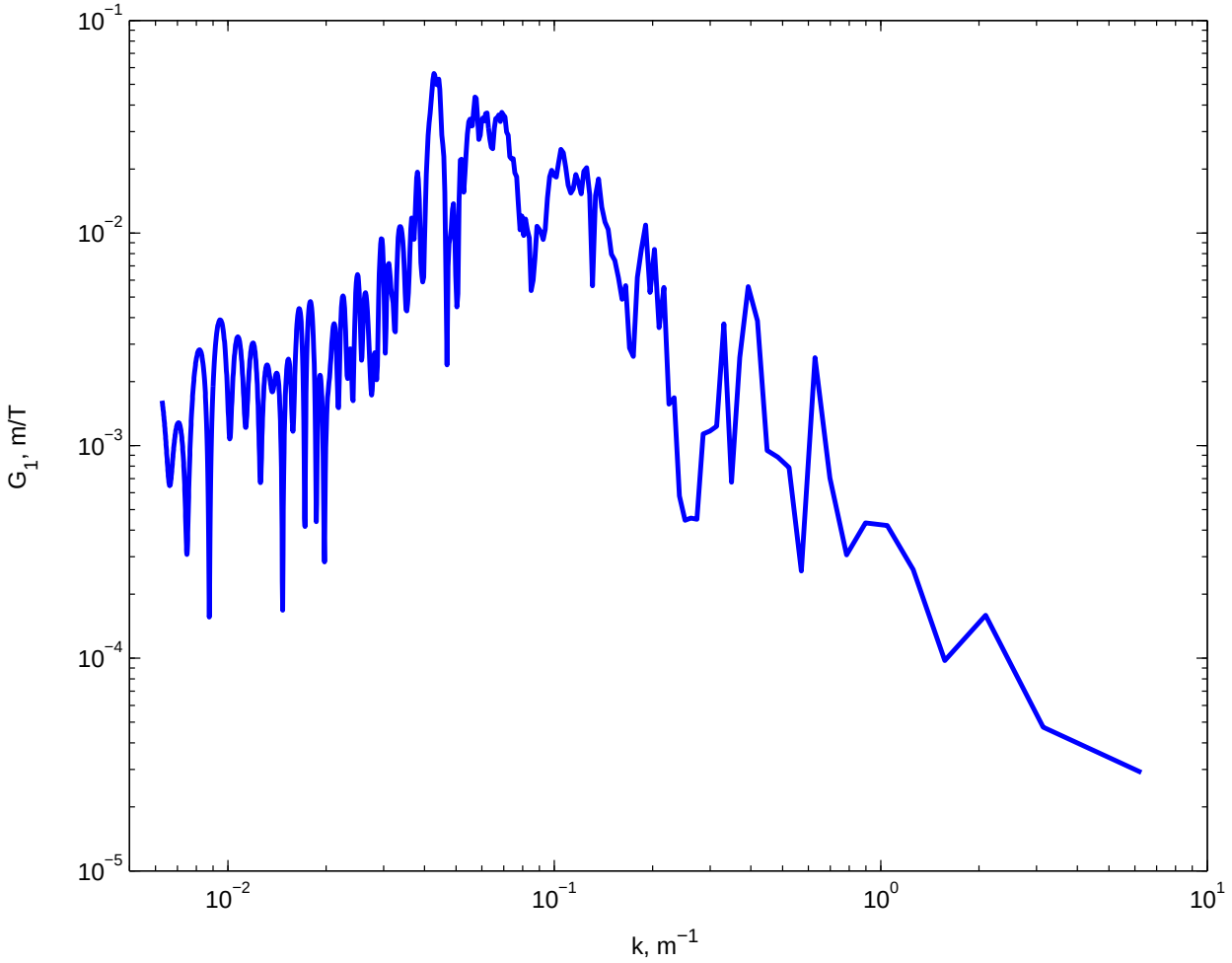

Figure 6: Sensitivity of IP beam position to a magnetic field with wave number k applied in the main linac.

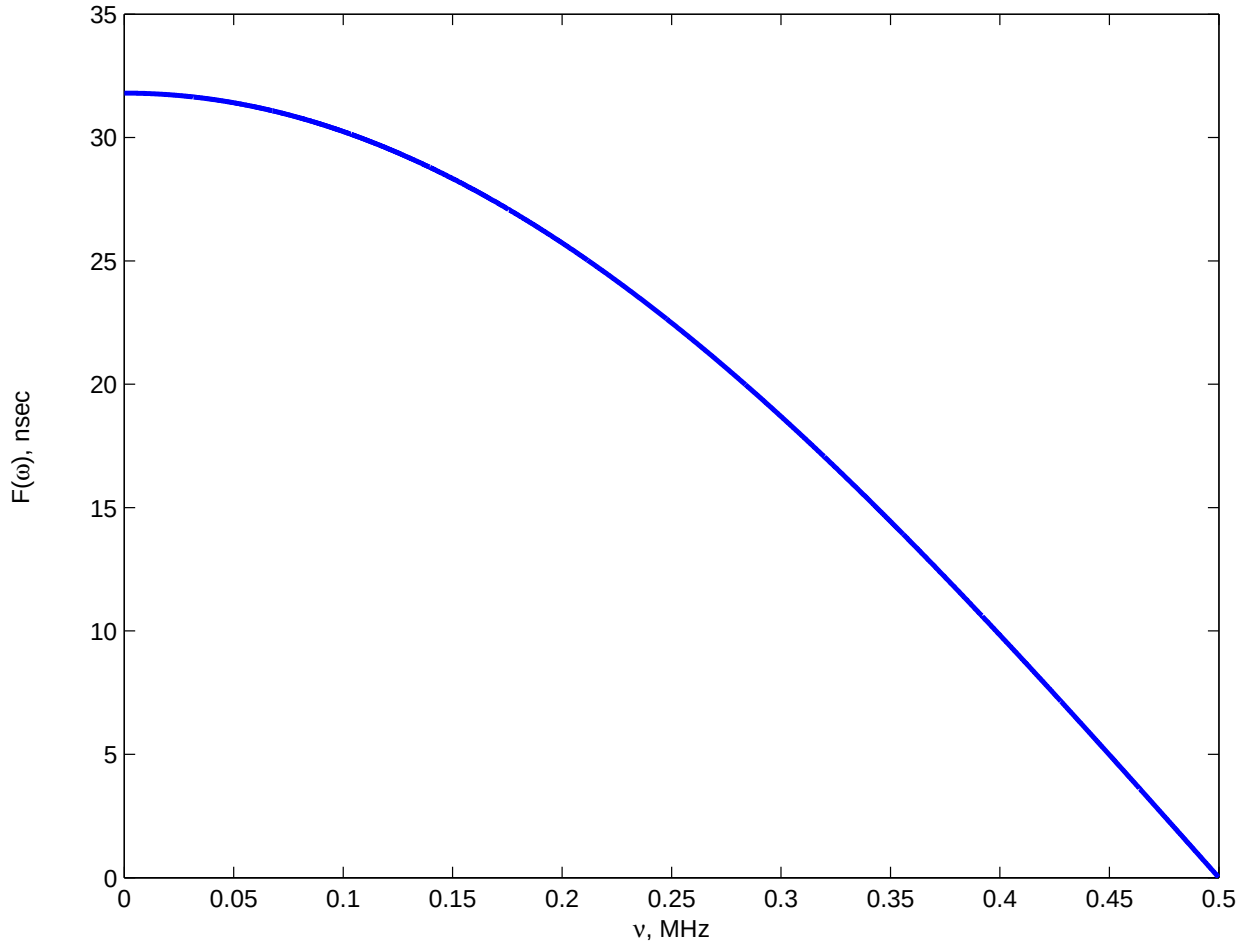

Figure 7: Fourier transform of a 2 μsec square pulse with unit height.

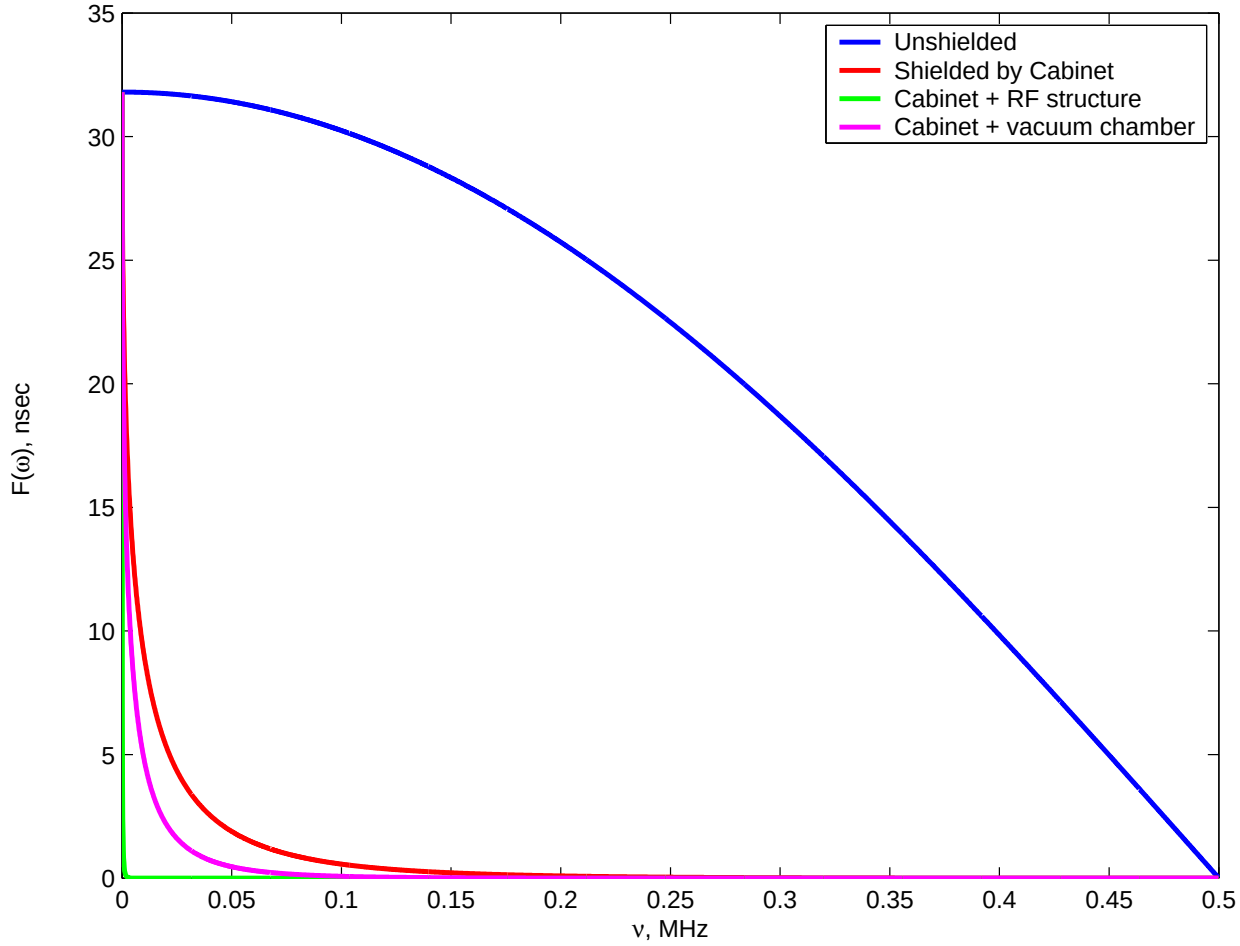

Figure 8: Frequency domain representation of 2 μsec square pulse with unit height, and same after filtering by the modulator cabinet, the cabinet plus an RF structure, the cabinet plus a steel vacuum chamber.

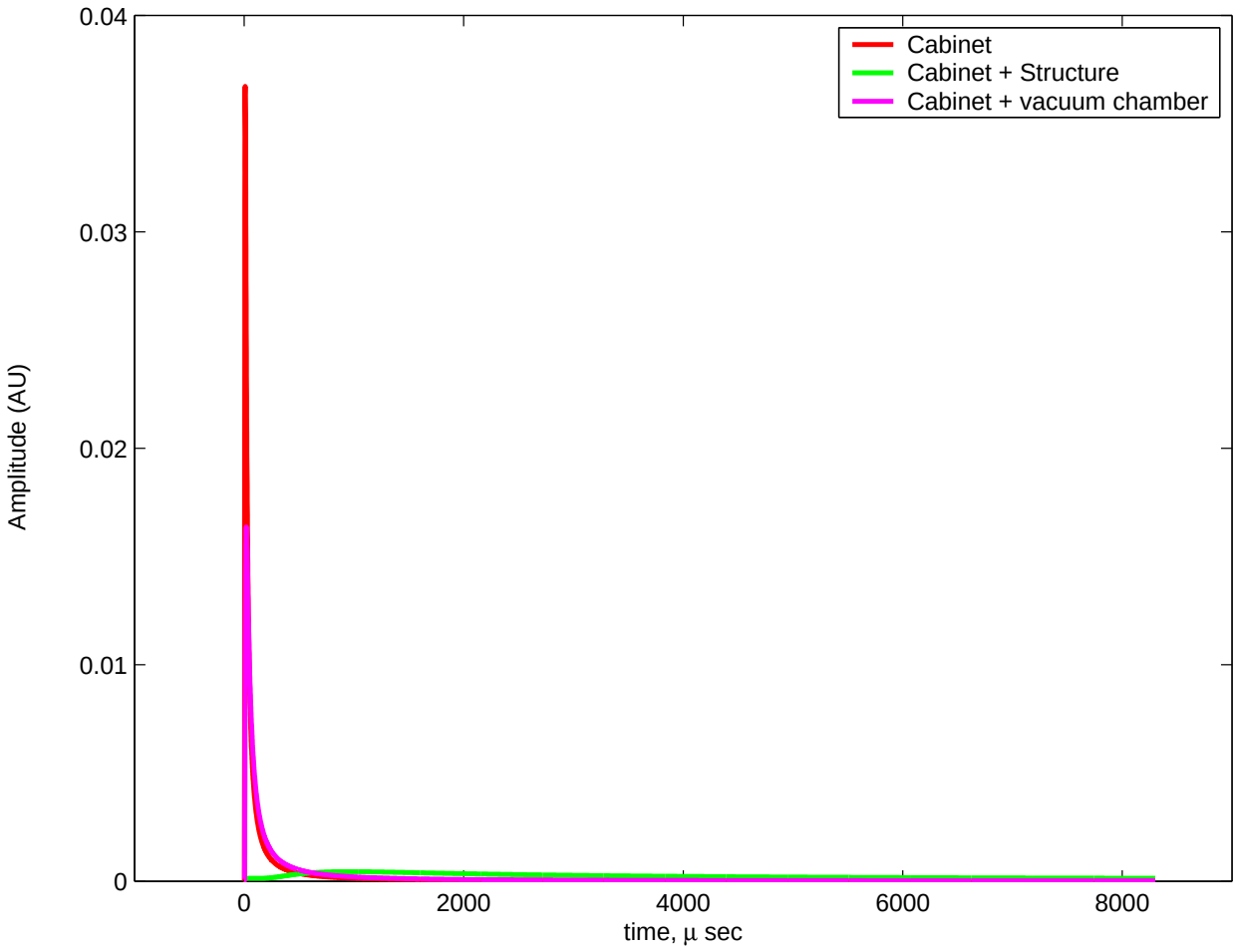

Figure 9: Time domain representation of 2 μsec square pulse with unit height, after filtering by modulator cabinet, by cabinet plus RF structure, and by cabinet plus steel vacuum chamber.

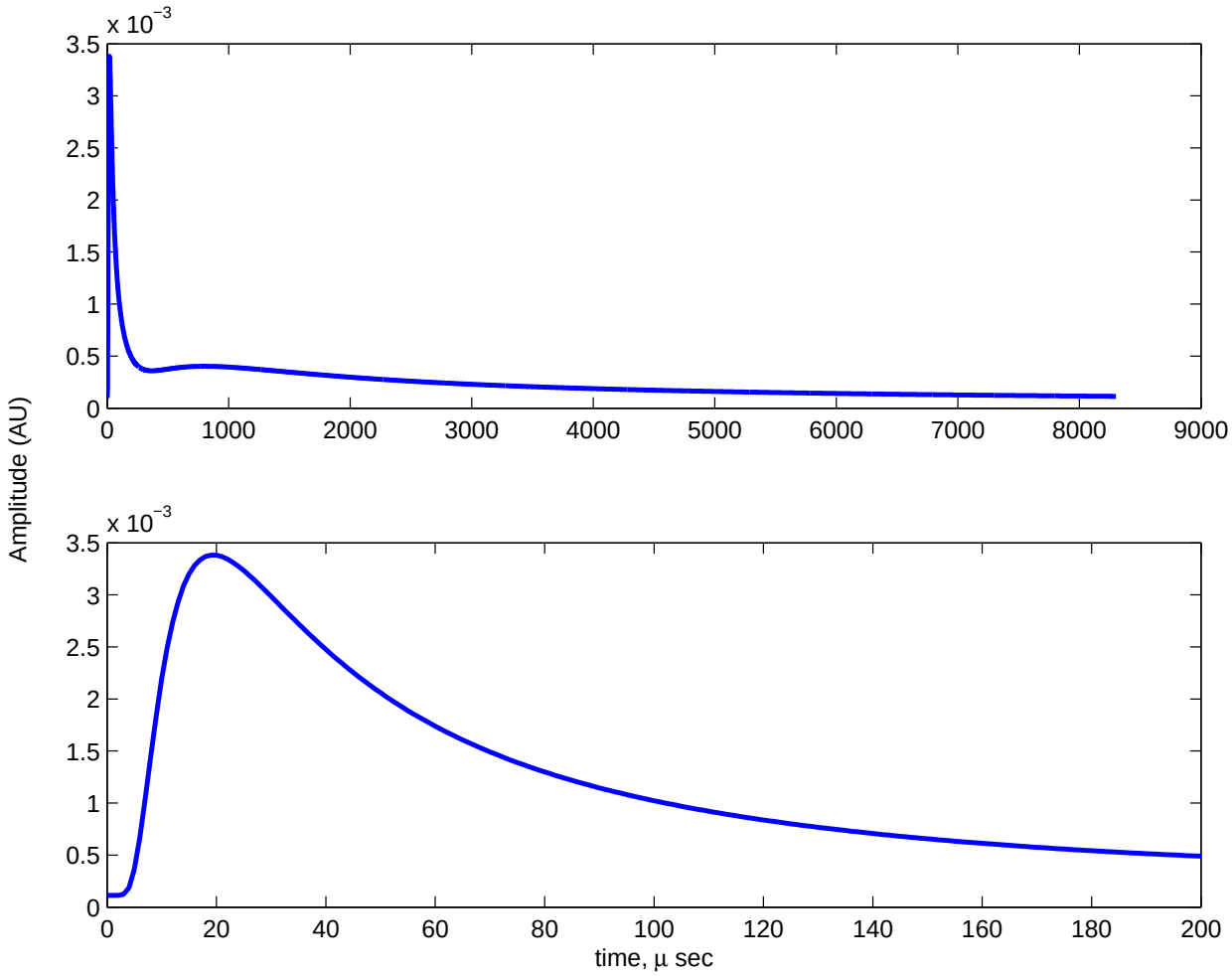

Figure 10: Time domain representation of the expected kick from a modulator pulse given the expected filtering in the NLC main linac, assuming 80% packing factor: both full length (top) and detailed view of first 100 μsec (bottom) are shown.

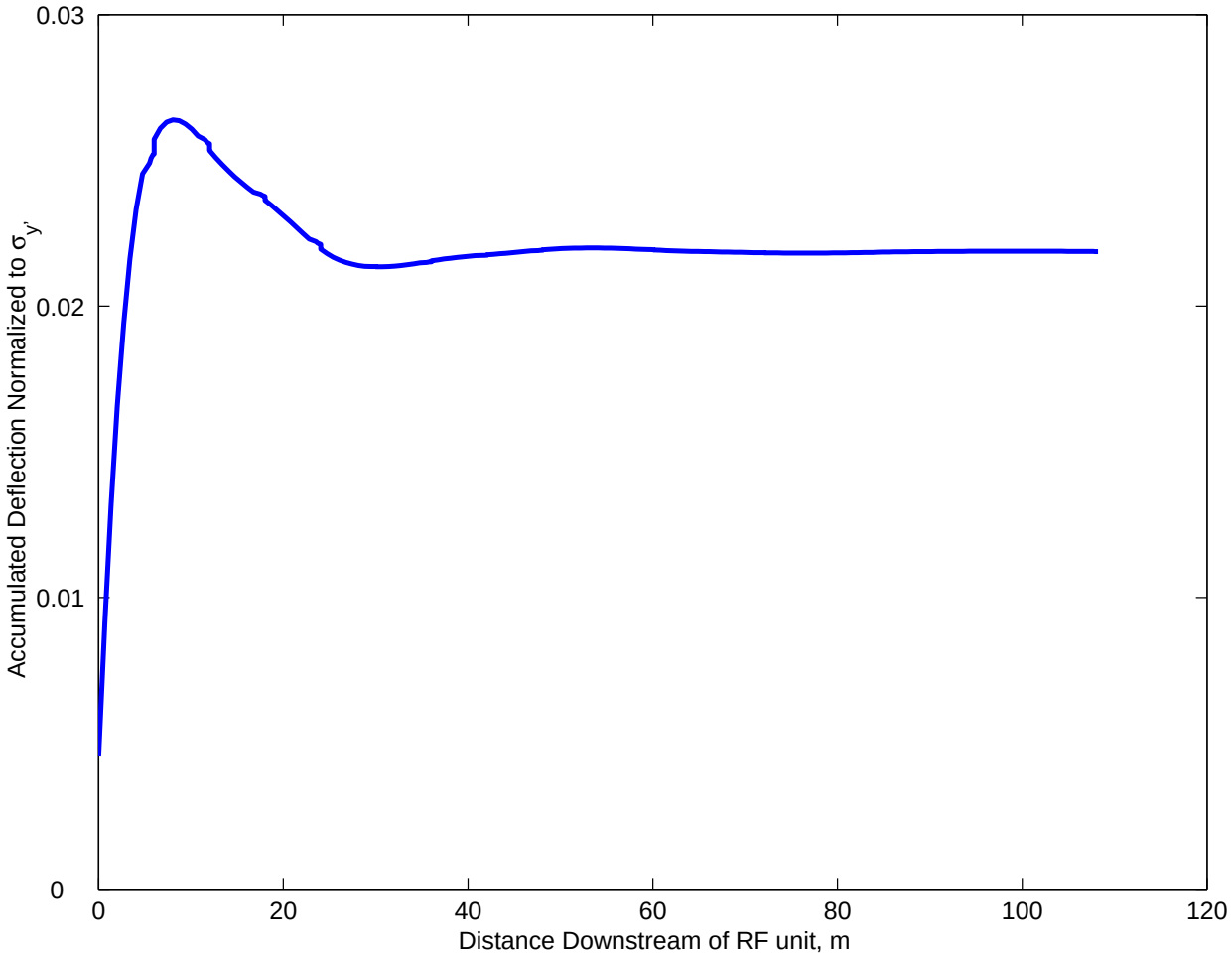

Figure 11: Cumulative kick to a 7.87 GeV beam in the NLC main linac from a modulator pulse, versus s position of the beam.

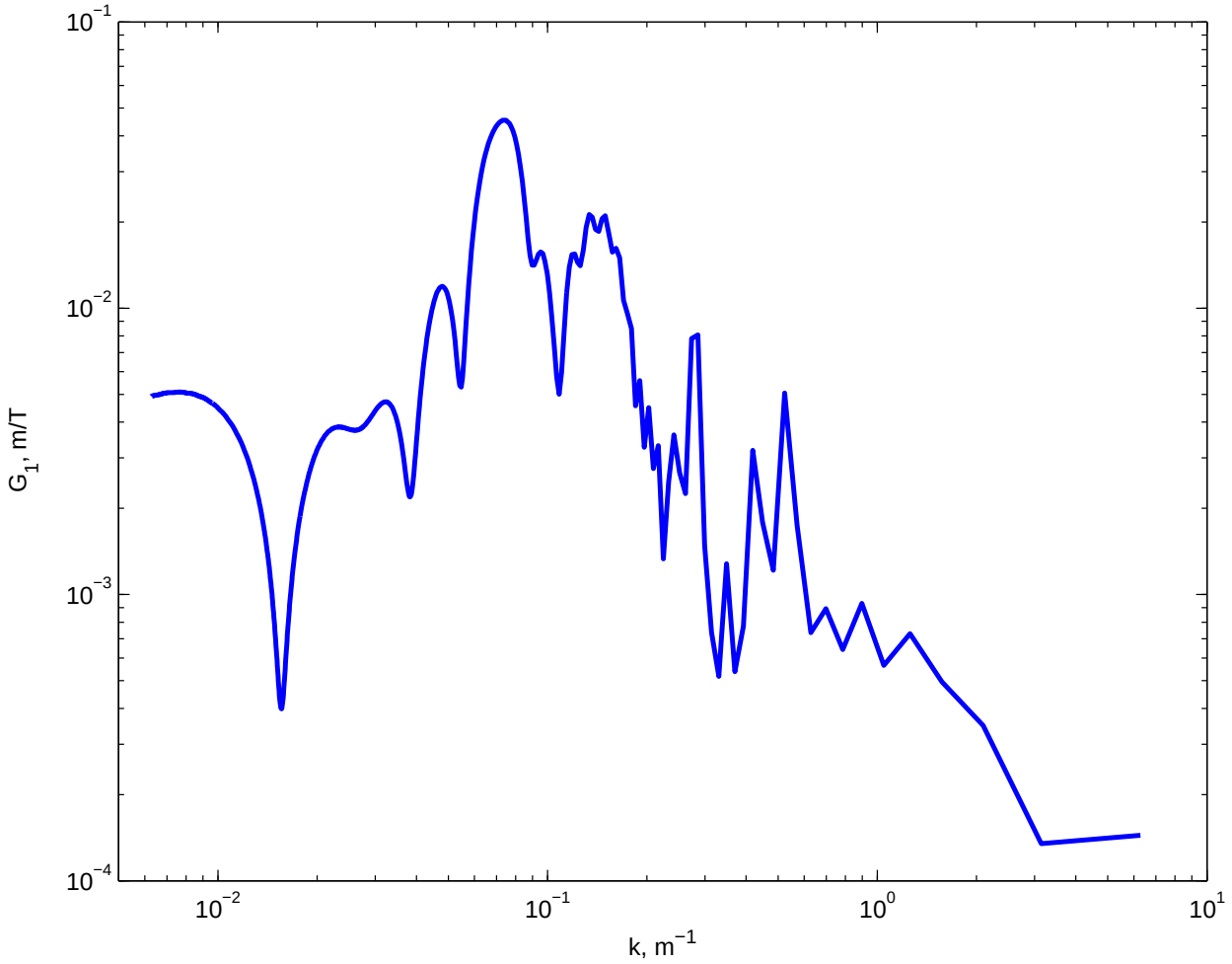

Figure 12: Sensitivity of IP beam position to a magnetic field with wave number k applied in the pre-linac.

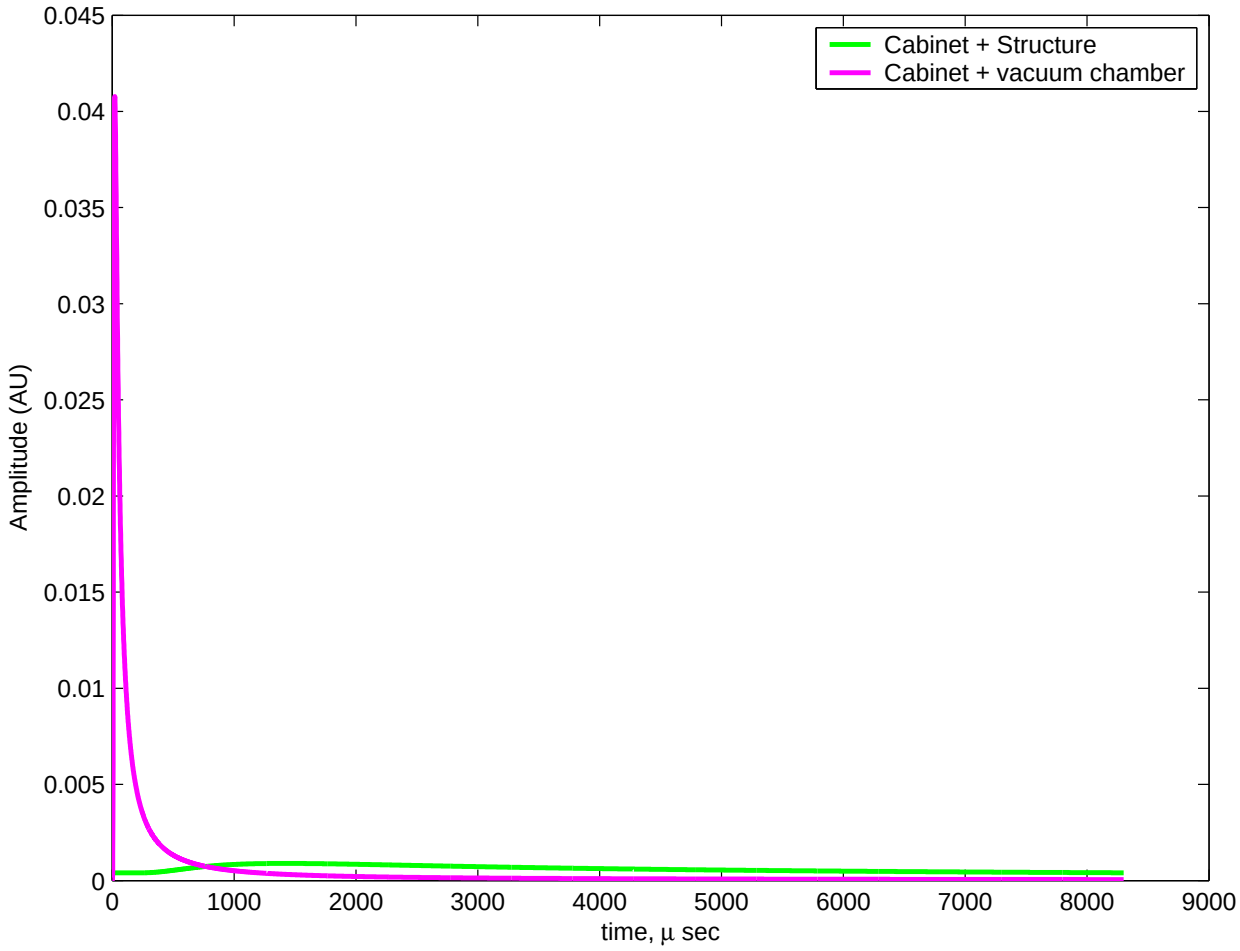

Figure 13: Field in the pre-linac from a modulator pulse, given various levels of shielding.

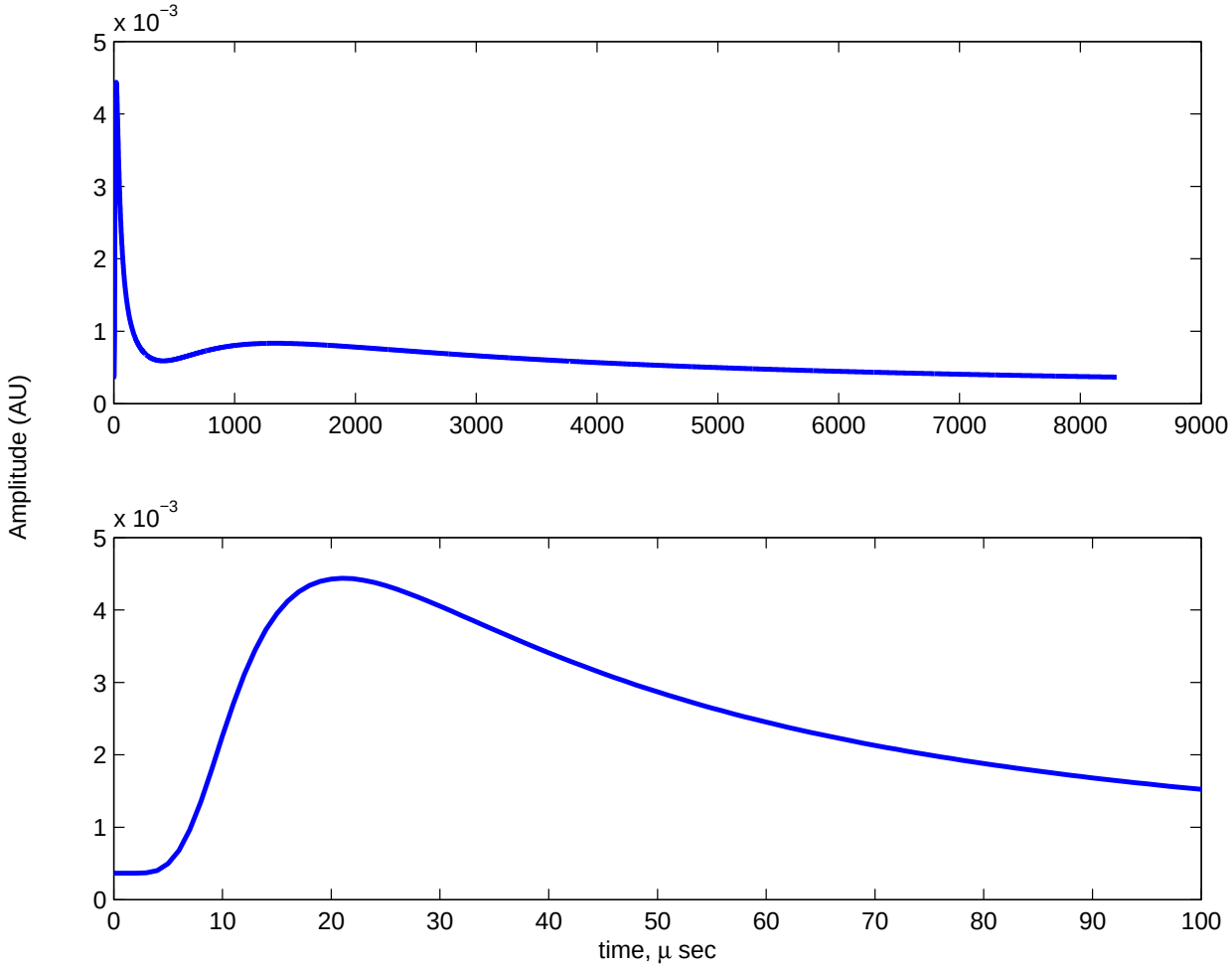

Figure 14: Average field in the pre-linac from a modulator pulse, given the expected 90% packing fraction: both full length (top) and detailed view of first 100 μsec (bottom) are shown.

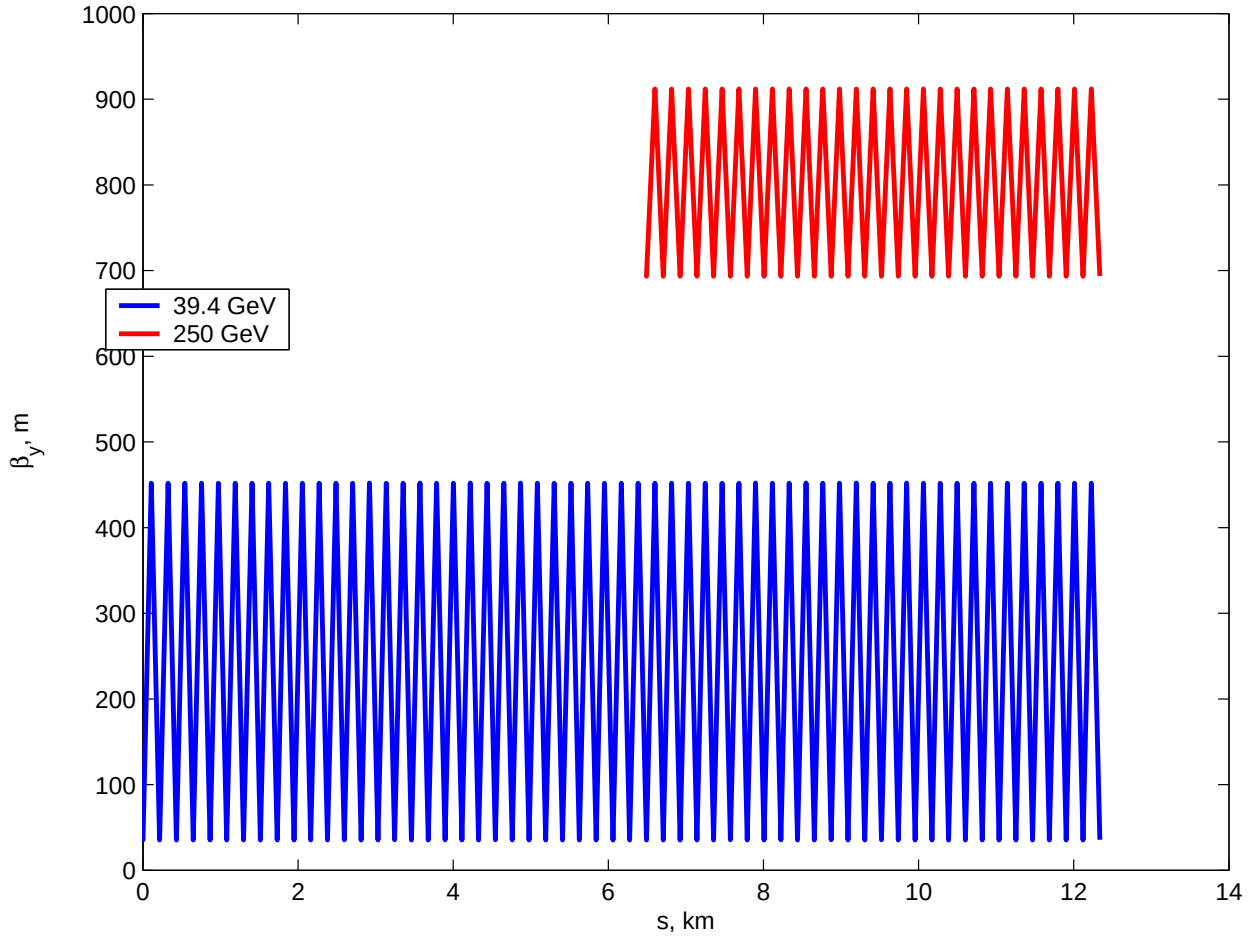

Figure 15: Optics of the main linac bypass line for 39.4 GeV beams (blue) and 250 GeV beams (red).

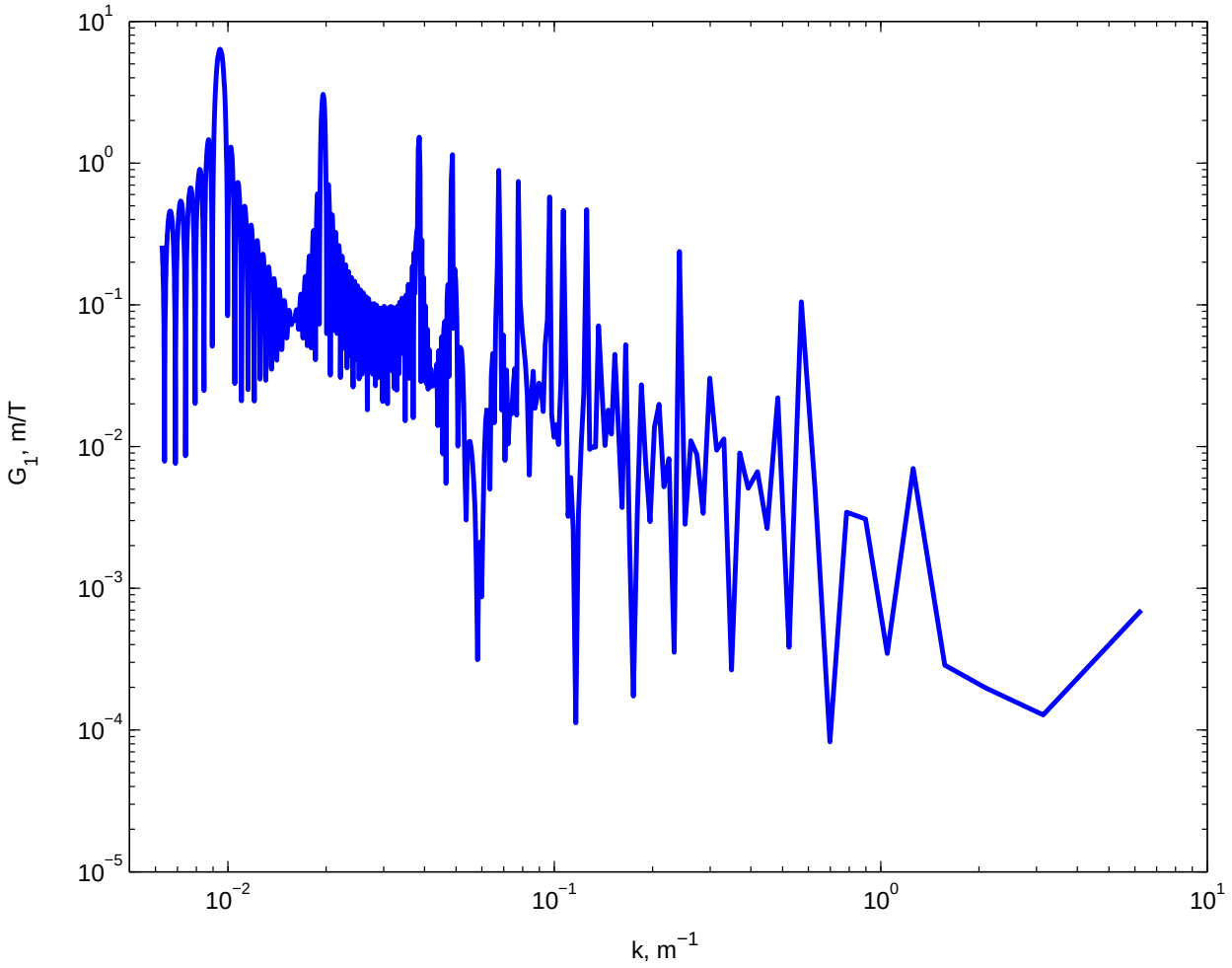

Figure 16: Sensitivity of IP beam position to a magnetic field with wave number k applied in the bypass line for 39.4 GeV configuration.

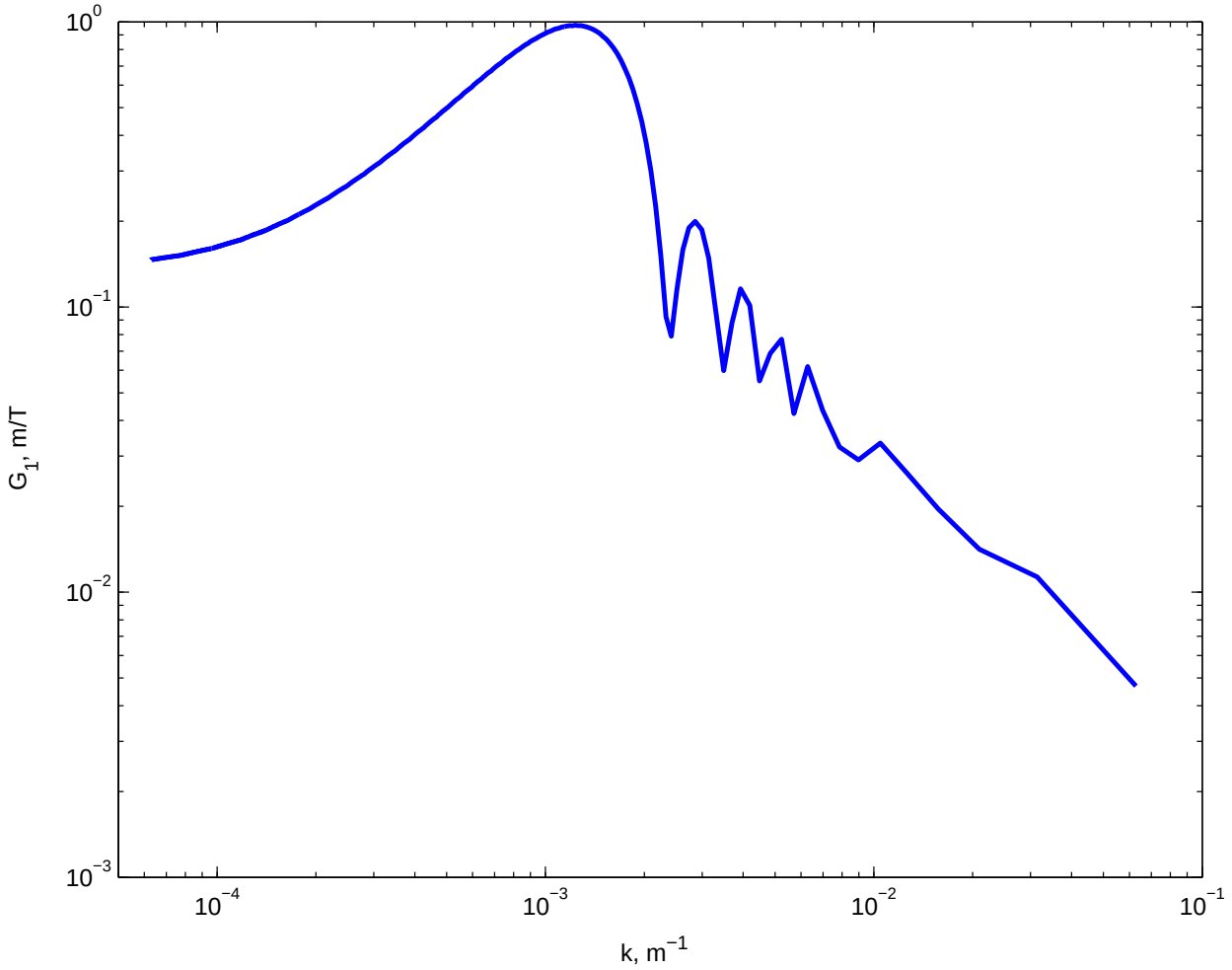

Figure 17: Sensitivity of IP beam position to a magnetic field with wave number k applied in the bypass line for 250 GeV configuration.